
^{11}C -JHU75528: A Radiotracer for PET Imaging of CB1 Cannabinoid Receptors

Andrew G. Horti, Hong Fan, Hiroto Kuwabara, John Hilton, Hayden T. Ravert, Daniel P. Holt, Mohab Alexander, Anil Kumar, Arman Rahmim, Ursula Scheffel, Dean F. Wong, and Robert F. Dannals

Department of Radiology, Johns Hopkins Medical Institutions, Baltimore, Maryland

The development of the radioligands for PET imaging of the cerebral cannabinoid receptor (CB1) is of great importance for studying its role in neuropsychiatric disorders, obesity, and drug dependence. None of the currently available radioligands for CB1 are suitable for quantitative PET, primarily because of their insufficient binding potential (BP) in brain or low penetration through the blood-brain barrier (BBB). The goal of this study was to evaluate ^{11}C -JHU75528, an analog of the selective CB1 antagonist rimonabant, in vivo as a potential CB1 radioligand for PET. **Methods:** The brain regional distribution and pharmacology of ^{11}C -JHU75528 have been evaluated in vivo in mice (dissection) and baboons (PET). **Results:** ^{11}C -JHU75528 readily entered the mouse and baboon brain and specifically and selectively labeled cerebral CB1 receptors. The ratio of striatum to brain stem in mice and the binding potential (BP) in the baboon putamen were 3.4 and 1.3–1.5, respectively. The specific binding of ^{11}C -JHU75528 in vivo was blocked by preinjection of nonlabeled JHU75528. Administration of rimonabant (1 mg/kg, intravenously) also blocked the specific binding of ^{11}C -JHU75528 in the mouse and baboon brain, whereas various central non-cannabinoid drugs did not significantly reduce the ^{11}C -JHU75528 binding in the mouse brain. ^{11}C -JHU75528 formed several hydrophilic metabolites, but only a minute fraction of metabolic radioactivity penetrated the BBB. **Conclusion:** ^{11}C -JHU75528 holds promise as a radiotracer with suitable imaging properties for quantification of CB1 receptors in the human brain.

Key Words: PET; cannabinoid receptor; ^{11}C -JHU75528

J Nucl Med 2006; 47:1689–1696

To date, 2 cannabinoid receptors have been characterized and cloned: CB1, predominantly located in the neural tissue and, to a lower extent, in the peripheral tissues; and CB2, which is found primarily in the peripheral tissues (1). Recent reviews summarize evidence that endocannabinoids and cannabinoid receptors play an essential role in many central and peripheral disorders (2–4). An altered regulation

of the cannabinoid system is found in depression schizophrenia and motor function disorders (2).

Findings from both clinical and preclinical studies suggest that ligands that block CB1 receptors offer a novel approach for treating patients with drug dependence. This approach may be efficacious across different classes of abused drugs, including alcohol, opiates, marijuana, and nicotine (5,6).

The administration of cannabinoid agonists leads to robust increases in food intake and can promote body weight gain in several species, including humans (7). In contrast, selective CB1 antagonists cause decreased appetite and are associated with weight loss when administered long term (7). The highly selective CB1 antagonist rimonabant (SR-141716; Acomplia [Sanofi-Aventis]) (8) has recently been found in phase III studies to significantly reduce body weight and waist circumference and to improve lipid and glucose metabolism in overweight and obese patients (9,10).

Despite the importance of the cannabinoid receptor system, the physiologic and pharmacologic roles played by these receptors in the central nervous system (CNS) are still not fully understood. The lack of radioligands for quantitative emission tomography imaging of cerebral cannabinoid receptors in humans represents a gap that hampers noninvasive research of the cannabinoid receptor system. Investigators have been attempting to fill this gap since the pioneering work on ^{18}F -labeled Δ^9 -THC (Δ^9 -tetrahydrocannabinol) in 1991 (11). Noninvasive imaging of the central CB1 receptor using PET would provide a great opportunity to study the role of CB1 in variety of disorders and for the development of cannabinergic medications. However, quantitative PET of CB1 in animal and human brain is still not possible, even though CB1 is abundant and displays high densities in the mammalian brain (1).

The existing PET/SPECT CB1 radioligands—mainly analogs of rimonabant and agonist WIN 55,212-2—exhibit high nonspecific binding that limits their application in PET and SPECT (11–22). At present, the in vivo radiotracers successfully used for imaging CNS receptors other than CB1 have lipophilicities in the range of $\log D_{7.4} = -1.5$ to $+4$. However, all currently available CB1 PET radiotracers display greater lipophilicity. A lipophilicity that is too high is often associated with increased nonspecific binding and, correspondingly, a low binding potential (BP), even when

Received Apr. 25, 2006; revision accepted Jun. 26, 2006.

For correspondence or reprints contact: Andrew G. Horti, PhD, PET Center, Division of Nuclear Medicine, Department of Radiology, Johns Hopkins Medicine, Nelson B1-151, 600 N. Wolfe St., Baltimore, MD 21287-0816.

E-mail: ahorti1@jhmi.edu

COPYRIGHT © 2006 by the Society of Nuclear Medicine, Inc.

the ligands have good binding affinity (23,24). Although the problem of high lipophilicity of CB1 radioligands is well recognized (13,15,18), it has not been fully resolved. An *in vivo* CB1 radiotracer with good binding affinity, lower lipophilicity, and, as a result, a better chance for reasonable imaging properties is still not available. To our knowledge, the best achieved ratio of target region to non-target region for the *in vivo* CB1 radiotracers was 2.5 in the mouse brain (for ^{18}F -SR144385) (13) and 1.5 in the rhesus monkey brain (for ^{11}C -NIDA41020) (25). The only reported attempt to quantify CB1 in the living human brain has demonstrated a low BP (0.2–0.3) of the radioligand ^{123}I -AM281 (21).

Another common problem with many previously developed PET radiotracers for imaging CB1 is poor permeability of the blood–brain barrier (BBB). A variety of molecular properties affect permeation of the BBB, including lipophilicity, hydrogen bonding capacity, molecular charge, size, shape, and flexibility. Although the influence of some of these factors is still unclear, it is well understood that optimal lipophilicity ($\log D_{7.4}$ between 1 and 4) is required for good BBB permeability (23,26). Therefore, insufficient brain uptake of many CB1 radioligands is not surprising because their lipophilicities ($\log D_{7.4} > 4$) are well above the conventional optimum for BBB permeability.

A very high lipophilicity is inherent to all cannabinoids because of their hydrophobic interaction with the receptor binding site. It is also influenced by the location of the binding site within the lipid bilayer of the cell membrane (27). A positive correlation between affinity and lipophilicity was demonstrated for 2 series of rimonabant analogs (15). This suggests that the design of a high-affinity CB1 radioligand with reduced lipophilicity and, as a result, a lower nonspecific binding and better BBB permeation is a challenge.

Our goal was to develop a CB1 ligand with a higher affinity and reduced lipophilicity. We recently synthesized JHU75528 (4-cyano-1-(2,4-dichlorophenyl)-5-(4-methoxyphenyl)-*N*-(piperidin-1-yl)-1H-pyrazole-3-carboxamide), a novel analog of rimonabant with a unique combination of higher binding affinity determined by inhibition binding assay with ^3H -CP55,940 and membranes from HEK-293 cells expressing the human recombinant CB1 receptor ($K_i^{\text{JHU75528}}/K_i^{\text{Rimonabant}} = 0.3$) and lower lipophilicity (experimental $\log D_{7.4} = 3.3$) than those of rimonabant (calculated $\log D_{7.4} = 6.0$) (28). In the same study, we radiolabeled JHU75528 with ^{11}C . Here we present the evaluation of ^{11}C -JHU75528 (4-cyano-1-(2,4-dichlorophenyl)-5-(4- ^{11}C -methoxyphenyl)-*N*-(piperidin-1-yl)-1H-pyrazole-3-carboxamide) as a potential PET radiotracer for quantitative *in vivo* imaging of cerebral CB1.

MATERIALS AND METHODS

Radiosynthesis of ^{11}C -JHU75528

^{11}C -JHU75528 was synthesized as described by our laboratory (28). Briefly, the radiotracer was prepared by radiomethylation of

the corresponding phenolic precursor. The final product was purified by high-performance liquid chromatography (HPLC) and formulated as a sterile apyrogenic solution in saline containing 9% alcohol. The specific activity of the tracer was in the range of 185–314.5 GBq/ μmol (5,000–8,500 mCi/ μmol), calculated at the end of synthesis, and the radiochemical purity exceeded 99%. The average radiochemical yield was 15% (nondecay corrected).

Biodistribution Studies in Mice

Baseline Study. Male CD-1 mice, weighing 25–30 g (Charles River Laboratories), were used for biodistribution studies. The animals were sacrificed by cervical dislocation at various times after injection of ^{11}C -JHU75528 (7.4–11.1 MBq [200–300 μCi]; specific radioactivity, ~ 111 GBq/ μmol [$\sim 3,000$ mCi/ μmol], in 0.2 mL saline) into a lateral tail vein. The brains were rapidly removed and dissected on ice. The brain regions of interest were weighed and their radioactivity content was determined in an automated γ -counter with a counting error below 3%. Aliquots of the injectate were prepared as standards and their radioactivity content was counted along with the tissue samples. The percentage injected dose per gram of tissue (%ID/g tissue) was calculated. All experimental protocols were approved by the Animal Care and Use Committee of the Johns Hopkins Medical Institutions.

Blocking with Rimonabant. *In vivo* CB1 receptor blocking studies were performed by intravenous administration of 2 mg/kg of rimonabant (SR141716) followed by intravenous injection of the radiotracer (7.4–11.1 MBq [200–300 μCi]; specific radioactivity, ~ 111 GBq/ μmol [$\sim 3,000$ mCi/ μmol]) 15 min thereafter. Rimonabant was dissolved in a vehicle solution (saline/alcohol/cremophore EL (9:1:0.06)) and administered in a volume of 0.1 mL. Control animals were injected with 0.1 mL of the vehicle solution. Ninety minutes after administration of the tracer, brain tissues were harvested, and the radioactivity content was determined.

Saturation of ^{11}C -JHU75528 Binding with JHU75528. *In vivo* saturation studies were done by intravenous administration of various doses of JHU75528 (0.08, 0.42, 0.78, and 4.17 mg/kg) followed by intravenous injection of the radiotracer (7.4–11.1 MBq [200–300 μCi]) 15 min thereafter. JHU75528 was dissolved in a vehicle (saline/alcohol/cremophore EL (9:1:0.01)) and administered in a volume of 0.1 mL. Control animals were injected with 0.1 mL of the vehicle solution. Sixty minutes after administration of the tracer, brain tissues were harvested, and their radioactivity content was determined.

CB1 Selectivity. *In vivo* receptor blocking studies were performed by intravenous administration of 0.1 mL of 6 noncannabinoid drugs shown in Table 1, followed by intravenous injection of the radiotracer (7.4–11.1 MBq [200–300 μCi]). Control animals were injected with 0.1 mL of isotonic saline. Sixty minutes after administration of the tracer, brain tissues were harvested, and their radioactivity content was determined as a %ID/g tissue normalized to the control in each region.

PET Studies in Baboon

General Design of PET Experiments. The experimental protocol was approved by the Animal Care and Use Committee of the Johns Hopkins Medical Institutions. Two male baboons (*Papio anubis*), 22 and 26 kg, were studied in baseline control ($n = 2$) and blocking ($n = 1$) experiments. The animals were fasted for

TABLE 1
Non-CB1 CNS Drugs for Blocking Studies in Mice

Non-CB1 drug	Target receptor	Dose (mg/kg)	Time of administration before radiotracer (min)
Naltrindole	Selective δ -opioid antagonist	3	5
Naloxone	μ -, κ -, δ -opioid antagonist	1	15
SCH23390	D ₁ - and D ₅ -antagonist and 5-HT _{1C/2C} agonist	1	5
Spiperone	D ₂ -like and 5-HT _{2A} receptor antagonist	1	5
Ketanserin	5-HT ₂ /5-HT _{2C} antagonist	2	5
Cytisine	$\alpha_4\beta_2$ -nAChR agonist	2	15

5-HT = 5-hydroxytryptamine (serotonin); nAChR = nicotinic acetylcholine receptor.

12 h before the PET study. Anesthesia was given initially with intramuscular injection of 20 mL (9 mg/kg) Saffan (alphadolone and alphaxalone mixture, 1:1) (Schering-Plough). The baboon was intubated and anesthesia was maintained with a constant infusion of Saffan diluted with isotonic saline (1:4) at an average flow rate that corresponded to 7.5 mg/kg/h. Circulatory volume was maintained by infusion of isotonic saline. An arterial catheter was inserted for blood sampling. Physiologic vital signs, including heart rate, electrocardiogram, blood pressure, and oxygen saturation were monitored continuously throughout the study.

The animal was positioned in a high-resolution research tomograph (ECAT HRRT) brain PET scanner (CPS Innovations, Inc.). The head of the baboon was fitted with a thermoplastic mask that was then attached to a head holder for reproducible fixation.

A 6-min transmission scan with a 37-MBq (1 mCi) ⁶⁸Ge source was initially performed for attenuation correction. Dynamic PET data were then acquired in 3-dimensional (3D) list mode during a 90-min period after a bolus injection of the radioligand in a list mode. Arterial blood was sampled rapidly initially and with prolonged intervals throughout the scan. Plasma samples taken at 0, 5, 30, 60, and 90 min were analyzed for metabolite as described.

The image reconstruction procedure consists of histogramming of the raw list-mode data into specified dynamic sinograms. The reconstruction of the attenuation density μ -map and segmentation of the μ -map were done, followed by calculation of attenuation factors using forward projection. The statistical 3D reconstruction of each frame sinogram uses 6 iterations of the OP-OSEM algorithm (Ordinary Poisson ordered subset expectation maximization; 16 subsets), followed by 2-mm gaussian postsMOOTHING. This is corrected for random coincidence events by application of iterative noise reduction/smoothing on the measured delayed coincidences and for scatter distribution using the Watson single-scatter simulation method. Application of dead time, decay, and calibration factor corrections was finally performed producing quantitative dynamic image sequences. The final frame schedule was used as follows: 4 × 15 s, 4 × 30 s, 3 × 60 s, 2 × 120 s, 5 × 240 s, and 12 × 300 s.

To analyze the PET images, the SPGR (spoiled gradient) MRI volume was acquired in the same baboon as the 76 transaxial images for anatomic identification of brain structures with the Signa 1.5-T scanner (GE Healthcare) using the following parameters: repetition time, 38 ms; echo time, 5 ms; flip angle, 45°; slice thickness, 1.5 mm with no gap; field of view, 24 × 18 cm; image acquisition matrix, 256 × 192, reformatted to 256 × 256.

PET Data Analysis. Volumes of interest (VOIs) were placed manually on SPGR MRI volumes for putamen, thalamus, cerebellum, and pons. Then, VOIs were transferred to PET space using MRI-to-PET alignment parameters that were obtained by manu-

ally aligning MR cortical outlines to averaged PET volumes (across 10- and 90-min frames) in 3D. In addition, a standard VOI template consisting of frontal, temporal, parietal, and occipital lobe VOIs was spatially transferred to an individual animal's PET space by applying standard-to-individual MRI spatial normalization parameters and MRI-to-PET alignment parameters. VOIs were applied to individual PET frames to obtain time-radioactivity curves (time-activity curves) of regions. The VOI drawing and coregistration tools were developed locally by one of the authors.

A preliminary study indicated that a 2-tissue, 1-vascular compartment model with 5 parameters described time-activity curves (the k_4 model with vascular volume). Thus, distribution volumes ($DV = K_1/k_2 (1 + k_3/k_4)$) of regions were estimated using the k_4 model with the following parameters: K_1 and k_2 are blood-brain and brain-blood clearance rate constants, respectively; k_3 is $B_{max} \cdot k_{on} \cdot f_2$, where B_{max} is the density of available CB1 receptors, k_{on} is the unidirectional association constant, and f_2 is the free fraction (i.e., not nonspecifically bound) of CB1 in the brain; k_4 is the unidirectional dissociation constant; and v_0 is the intratissue vascular volume. To reduce the number of model parameters to estimate, the K_1/k_2 value was fixed at the pons value to estimate the remaining parameters in other regions (29,30). Assuming that the minute amounts of metabolites of ¹¹C-JHU75528 that enter the brain do not bind to the CB1 receptor, metabolite-corrected plasma and time-activity curves were used for model parameter estimation except that the total plasma time-activity curve was used to calculate the intravascular radioactivity in regions. Regional values of BPs were calculated as DV ratio minus 1 ($DV/DV^R - 1$, where DV^R is distribution volume of the reference region). The pons was selected as a reference region. Regional BP values were also obtained by the multilinear reference tissue method with 2 parameters (MRTM2) (31). Regional changes of BP after blocking were calculated as $1 - BP_B/BP_C$, where subscripts C and B refer to control and blocking PET experiments, and expressed as percentage.

Control PET Studies. Two control studies in the baboon were done. A sterile apyrogenic solution (3 mL) of ¹¹C-JHU75528 (625.3 and 1,110 MBq [16.9 and 30 mCi]; 188.7–199.8 GBq/ μ mol [5,100–5,400 mCi/ μ mol]) in isotonic saline containing 9% alcohol was injected intravenously as a bolus, followed by PET immediately after the administration.

Blocking with Rimobant. Immediately after the completion of the first control experiment, a dose of 1 mg/kg rimobant in a vehicle of saline/alcohol/cremophore EL (10:1:0.06) was given intravenously and ¹¹C-JHU75528 (603.1 MBq [16.3 mCi]; 276.4 GBq/ μ mol [7,470 mCi/ μ mol]) was injected 15 min after administration of the blocker.

Analysis of Metabolites

Baboon Plasma. Metabolites of ^{11}C -JHU75528 in the baboon were studied using a general method developed previously for PET radiotracers (32). Specifically, arterial blood samples were withdrawn at 5, 15, 30, 60, and 90 min after injection and plasma was analyzed for the presence of ^{11}C -JHU75528 and its radiolabeled metabolites. Briefly, 3 mL plasma in 8 mol/L urea acidified with 50 mg citric acid is passed through a capture column (Strata-X, 19×4.6 mm; Phenomenex) at 2 mL/min, followed by 1% acetonitrile in water to wash plasma proteins from the column. The effluent from the capture column, containing only highly polar components, flows through a dual bismuth germanate detector (Bioscan). The solvent is then switched to 65% acetonitrile in 10 mmol/L sodium phosphate buffer, pH 5.5 (2 mL/min), for elution of the radiolabeled components bound to the capture column onto the analytic column (Synergi Polar-RP, 10 μm , 250×4.6 mm; Phenomenex).

Mouse Plasma and Mouse Brain. Male CD-1 mice were injected intravenously with 111 MBq (3 mCi) ^{11}C -JHU75528 in 0.2 mL saline. Whole brain and heparinized blood were harvested at 10, 20, and 30 min after the injection of radiotracer. Mouse blood and brain extract were analyzed by the method described for the baboon blood analysis. Each brain was homogenized in 1 mL of acetonitrile and the homogenate was centrifuged for 5 min in a microcentrifuge. An aliquot of the supernatant was diluted with water and analyzed by HPLC as described.

RESULTS

Biodistribution Studies in Mice

The initial in vivo evaluation of ^{11}C -JHU75528 was performed in mice. The brain uptake of ^{11}C -JHU75528 was high. The time-activity curves of ^{11}C -JHU75528 in cerebellum, hippocampus, striatum, cortex, brain stem, and thalamus (Fig. 1) show the peak concentration of radioactivity in all regions at 15–20 min followed by washout. The highest accumulation of ^{11}C radioactivity occurred in the striatum ($6.6\% \pm 0.7\%$ ID/g tissue [mean \pm SD of 3]), hippocampus, cortex, and cerebellum, and the lowest radioactivity occurred in the brain stem and thalamus. The clearance rate of ^{11}C -JHU75528 from the thalamus and brain stem was

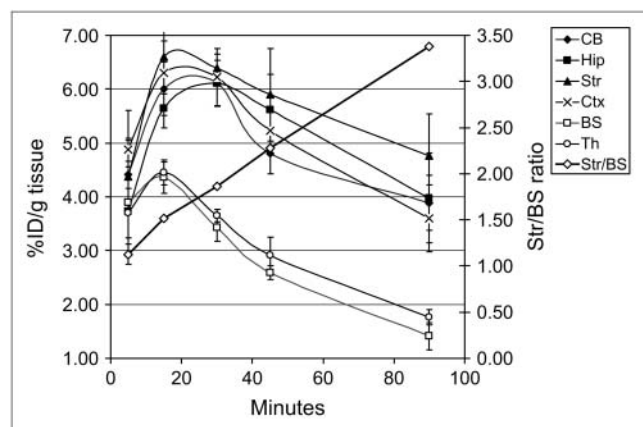


FIGURE 1. Regional brain distribution of ^{11}C -JHU75528 in mice. CB = cerebellum; Hip = hippocampus; Str = striatum; Ctx = cortex; BS = brain stem; Th = thalamus.

higher than that from any other region studied. The ratios of tissue to brain stem increased steadily over the observation period, reaching values of 3.4 in the striatum and 2.8 in the hippocampus and cerebellum at 90 min after injection (Fig. 1).

A blocking dose of the selective CB1 antagonist rimonabant significantly inhibited ^{11}C -JHU75528 binding at 90 min after administration of the tracer in all regions of the mouse brain examined, except the thalamus, a region with a low density of CB1 (Fig. 2).

To study saturation of the radiotracer binding, we injected unlabeled JHU75528 before administration of the radioligand (Fig. 3). The observed reduction of radioactivity after JHU755280 administration was greater in the regions with higher density of CB1 than that in the CB1-poor thalamus. When specific binding was estimated by using the radioactivity concentration in the blocked thalamus as nonspecific binding in the hippocampus and striatum, the decrease in these brain regions amounted to 84%. Importantly, the blocking doses of JHU755280 and rimonabant did not produce visible pharmacologic effects in mice.

For determination of the selectivity of ^{11}C -JHU75528 toward CB1 receptors versus several major cerebral receptor systems, we compared the regional biodistribution of the radiotracer in control mice with that in mice preinjected with various CNS active drugs (Table 1). The choice of the drugs was dictated by the interaction of CB1 receptors with the receptor systems of these drugs (1) and the recent data suggesting that CB1 antagonists are promising medications for treatment of dependence to various classes of non-cannabinoid narcotics (5,6). None of the drugs injected before administration of the radiotracer significantly reduced accumulation of radioactivity when compared with that of the control animals, suggesting that these drugs did not compete with ^{11}C -JHU75528 for the binding sites. However, injection of spiperone significantly increased accumulation of radioactivity in the striatum and brain stem and injection

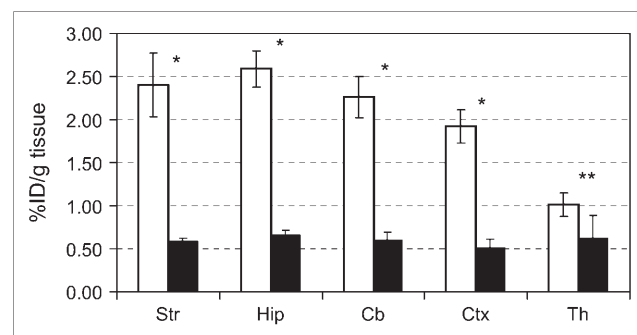


FIGURE 2. Comparison of regional brain uptake of ^{11}C -JHU75528 in mice at 90-min time point in control (white bars) and blocking experiments with rimonabant (1 mg/kg) (black bars). There was significant blocking in all regions except thalamus. Str = striatum; Hip = hippocampus; Cb = cerebellum; Ctx = cortex; Th = thalamus. Data are mean \pm SD. * $P < 0.001$, significantly different from controls; ** $P = 0.09$, insignificantly different from controls (ANOVA single-factor analysis).

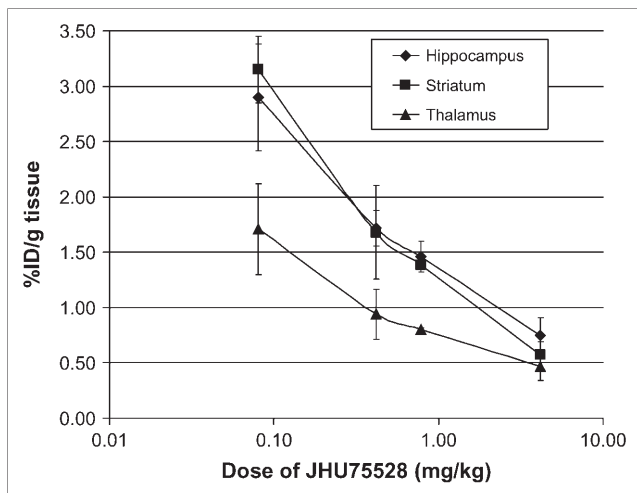


FIGURE 3. Saturation of inhibition of ^{11}C -JHU75528 accumulation by intravenous preinjection of unlabeled JHU75528 (0.08, 0.42, 0.78, and 4.12 mg/kg) in different regions of mouse brain 60 min after injection of radiotracer. Data are mean \pm SD, 3 animals per concentration.

of ketanserin and cytisine increased accumulation of radioactivity in the hippocampus and striatum, correspondingly (Fig. 4).

PET Studies in Baboon

A robust incorporation of radioactivity into the baboon brain (Figs. 5 and 6) was seen in a baseline PET study after injection of ^{11}C -JHU75528. Like the results of our mice studies, the pattern of radioactivity distribution in baboon brain is comparable with the distribution of CB1 that was found in previous autoradiographic experiments (33,34)

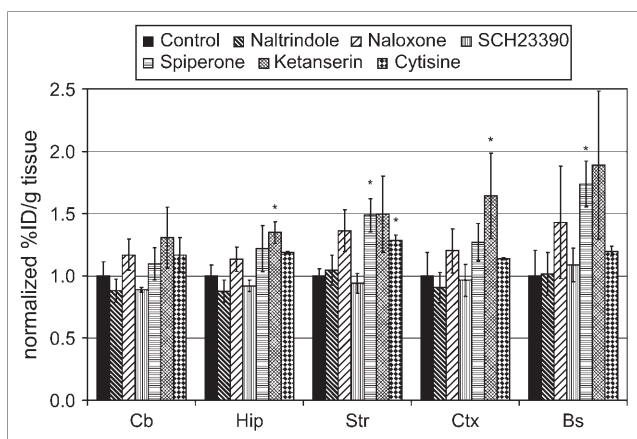


FIGURE 4. Effect of central drugs on accumulation of ^{11}C -JHU75528 in mouse brain regions 60 min after injection of tracer expressed as %ID/g tissue normalized to control in each region. Cb = cerebellum; Hip = hippocampus; Str = striatum; Ctx = cortex; Bs = brain stem. Data are mean \pm SD of 3 mice. * $P < 0.05$, significantly different from controls. Columns that do not include the asterisk are insignificantly different from controls ($P > 0.05$) (ANOVA single-factor analysis).

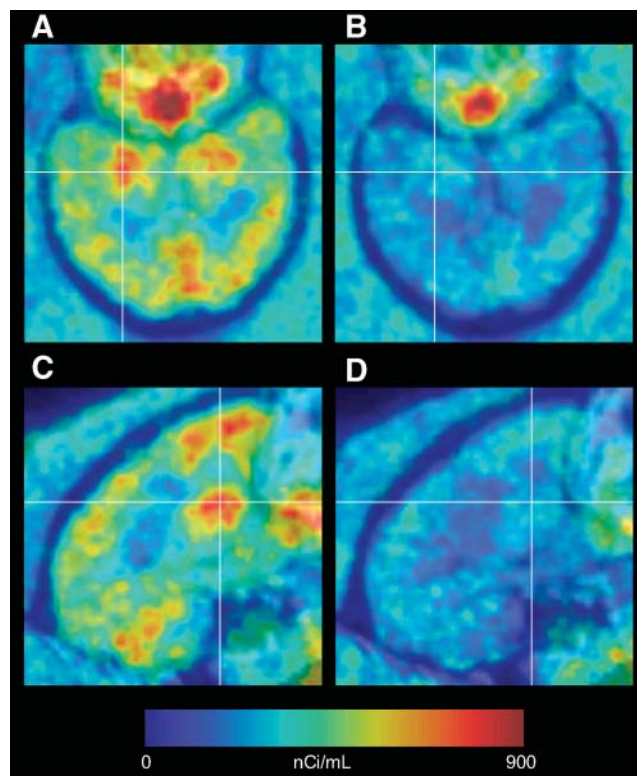


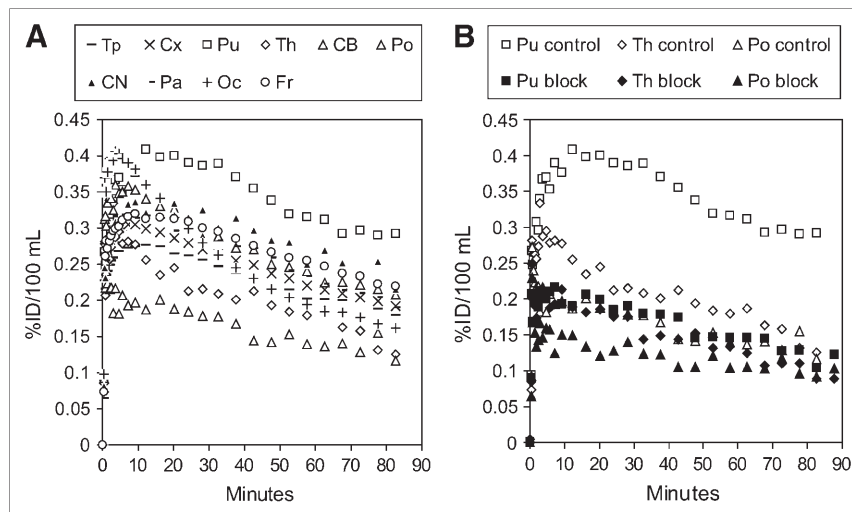
FIGURE 5. Averaged baboon PET images (frames taken between 10 and 90 min) of ^{11}C -JHU75528 scans, displayed on aligned MR images. Lines cross at center of left putamen. Images are shown in same color scale (Bq/mL [nCi/mL]). (A) Transaxial image, baseline. (B) Transaxial image, blocking with rimonabant (1 mg/kg, intravenously). (C) Sagittal image, baseline. (D) Sagittal image, blocking with rimonabant. Transaxial images display putamen, thalamus, and temporal and occipital cortices. Sagittal images display putamen, frontal, parietal, and occipital cortices, and cerebellum, among other structures. On baseline scan, radioactivity accumulated predominantly in putamen, frontal cortex, and cerebellum, and less in thalamus and pons.

and PET/SPECT (19,20,25) data. The ratios of putamen to thalamus and putamen to pons increased over the 90-min observation period, reaching a high for the CB1 receptor values of 2.2 and 2.5, respectively.

Similar to the blocking results in mice, injection of rimonabant (1 mg/kg, intravenously) dramatically reduced the regional radioactivity uptake in the baboon brain regions with high and intermediate densities of CB1, whereas little displacement of radioactivity from the CB1-poor thalamus and pons was observed (Figs. 5 and 6). This result suggests that the thalamus or pons may be used as reference regions for mathematic modeling. We did not notice any significant changes in the vital signs of the baboon when either the tracer dose of ^{11}C -JHU75528 or the blocking dose of rimonabant was injected.

High extracerebral uptake of ^{11}C -JHU75528 within the anterior basal portion of the baboon skull (Fig. 5A) was significantly blocked by the administration of rimonabant (Fig. 5B). This suggests that the presence of CB1 in that

FIGURE 6. Data obtained from PET study in baboon that demonstrates imaging of CB1 with ^{11}C -JHU75528. Tp = temporal lobe; Cx = cortex; Pu = putamen; Th = thalamus; CB = cerebellum; Po = pons; CN = caudate nucleus; Pa = parietal lobe; Oc = occipital lobe; Fr = frontal lobe. The record high ratio of accumulated radioactivity in CB1-rich regions vs. CB1-poor regions ($\text{Pu/Po} = 2.5$) suggests that tracer could be used successfully in PET studies. (A) Regional brain time-activity curves of ^{11}C -JHU75528 (bolus, 625.3 MBq [16.9 mCi]; specific radioactivity, 199.8 GBq/ μmol [5,400 mCi/ μmol]) in male baboon (26 kg). (B): Putamen and thalamus time-activity curves of ^{11}C -JHU75528 in same male baboon as in A in a control and a blockade study (1 mg/kg rimonabant, intravenously, 15 min before radiotracer injection; radiotracer: bolus, 603.1 MBq [16.3 mCi]; specific radioactivity, 277.5 GBq/ μmol [7,470 mCi/ μmol]).



area corresponds, perhaps, to bone marrow. Previous studies have demonstrated the presence of messenger RNA of the CB1 receptor in various peripheral tissues, including bone marrow (1).

Mathematic modeling of radiotracer distribution in the baboon brain with the pons taken as a reference region demonstrated that the highest BP value was in the putamen (1.3) followed by the caudate nucleus (0.85) and the frontal lobe (0.74). The lowest values were observed in the occipital lobe (0.26) and the thalamus (0.09) (Fig. 7A). Blocking with rimonabant caused greater reduction of the regional values of BP in the putamen, caudate nucleus, and cerebellum as compared with those in the occipital cortex and thalamus (Fig. 7B). We found a good correlation of regional BP values of the reference region approach (y) to regional BP values of the k4-model approach (x) with metabolite-corrected plasma inputs ($y = 0.74x + 0.19$; $R^2 = 0.974$) ($\text{BP}^{\text{Putamen}} = 1.5$).

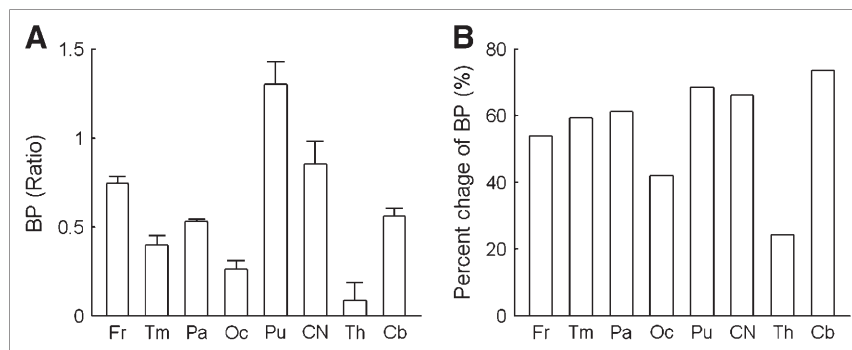
HPLC metabolite analysis of blood samples from mice and baboon showed that ^{11}C -JHU75528 undergoes metabolism with a moderate rate of conversion of the parent compound to 5 hydrophilic metabolites. These metabolites

appear to poorly penetrate the BBB. Thus, 94% of unchanged parent compound was present in the mouse brain versus 19% in the blood in 30 min after intravenous administration of ^{11}C -JHU75528. The major part of this minute amount of radiolabeled metabolites in the mouse brain seen on a reverse-phase HPLC chromatogram (not presented) corresponds to a wide peak having a retention time of the void volume of the capture column. This peak is typical of metabolites of ^{11}C -arenes such as ^{11}C -DTBZ ($(\pm)\text{-}\alpha\text{-}^{11}\text{C}$ -dihydro-tetra-benzazine) or ^{11}C -L-159884 (32) and is likely to correspond to ^{11}C - CO_2 (35). ^{11}C - CO_2 is excreted primarily through the lungs and only partially penetrates the BBB (36).

DISCUSSION

Previous in vitro studies demonstrated that our novel cannabinoid radioligand JHU75528 exhibits a unique combination of high binding affinity and a lipophilicity value that is in the optimal range for BBB permeability. We expected that ^{11}C -JHU75528 would enter the brain and would display good specific binding and, because the tracer

FIGURE 7. (A) Mean regional BP values \pm SD ($n = 2$). (B) Percent changes in BP of baboon brain regions after blocking with rimonabant. Fr = frontal lobe; Tm = temporal lobe; Pa = parietal lobe; Oc = occipital lobe; Pu = putamen; CN = caudate nucleus; Th = thalamus; Cb = cerebellum.



lipophilicity is lower than those of currently known CB1 radioligands, relatively low nonspecific binding.

As we expected, the *in vivo* distribution studies with ^{11}C -JHU75528 in mice (Fig. 1) demonstrated high uptake of radioactivity in the striatum, hippocampus, cortex, and cerebellum and lower uptake in the thalamus and brain stem. This distribution of ^{11}C radioactivity matches the distribution of CB1 in mammalian brain (33,34), providing evidence that ^{11}C -JHU75528 binds *in vivo* with CB1 receptor. To our knowledge, the ratios of target to brain stem obtained from this distribution study in mice are the highest reported to date for *in vivo* CB1 radioligands. The shape of the ratio–time curve in mice (Fig. 1) suggests that the maximum value of the ratio has not been reached during the 90-min observation period.

After injection of ^{11}C -JHU75528 in the baboon, the radioactivity was distributed heterogeneously, which also matched the previously published distribution of the CB1 receptor in autoradiographic studies (33,34). Radioactivity reached its peak at about 10 min after injection, and the binding was reversible (Fig. 6). The ratio of target to nontarget (ratio of putamen to brain stem = 2.5) was high for a CB1 radiotracer.

The successful blocking of the accumulation of ^{11}C -JHU75528 radioactivity in mice and baboon with the selective CB1 antagonist rimonabant demonstrated that ^{11}C -JHU75528 uptake in the receptor-rich regions of the brain is CB1 mediated (Figs. 2, 5, and 6). In addition, the blockade of the ^{11}C -JHU75528 binding with nonlabeled JHU75528 in the saturation experiments suggested that the binding of the radiotracer is specific.

We did not observe side effects in mice injected intravenously with nonlabeled JHU75528 in the doses up to 4.3 mg/kg. This result suggests a low acute toxicity of JHU75528 in mice.

The *in vivo* CB1 selectivity of ^{11}C -JHU75528 was studied in the experiment involving several non-CB1 CNS drugs. Preadministration of these drugs did not significantly reduce the accumulation of radioactivity in the brain regions compared with the control experiment (Fig. 4). The reason for the increase of uptake of ^{11}C -JHU75528 in several brain regions in the presence of spiperone, ketanserin, and cytosine is unclear. However, such effects of CNS drugs are not uncommon and have been attributed to added tracer availability from the periphery or blood flow changes (13).

HPLC analyses of mouse and baboon plasma indicate that in both species ^{11}C -JHU75528 forms the same radioactive metabolites, including $^{11}\text{CO}_2$. However, only a small amount of radioactivity other than the parent compound was found in the mouse brain. This result suggests that for quantification of the CB1 receptor with ^{11}C -JHU75528, PET metabolite modeling is not necessary.

Mathematic modeling of ^{11}C -JHU75528 in the baboon brain revealed a BP value in putamen (BP = 1.3–1.5) that is comparable with that of many CNS receptor radiotracers that are currently in use for quantitative PET studies. ^{123}I -

AM281, the only available radioligand for imaging of CB1 receptors in the human brain by emission tomography, exhibits a lower value of BP (0.2–0.3) in the target organ (21). Further test–retest and PET modeling studies with ^{11}C -JHU75528 in baboon are warranted.

In brief, ^{11}C -JHU75528 manifests reasonable properties for quantitative imaging of CB1 in the human brain. The main advantage of ^{11}C -JHU75528 as an *in vivo* radiotracer is a good signal-to-noise ratio. In addition to CB1 receptor imaging of different classes of abused drugs (5,6), ^{11}C -JHU75528 can be used potentially as a PET radioligand for studying CB1 receptors in disorders when altered regulation of the CB1 system is found (2). Good BP values in the baboon brain suggest that the radiotracer can be used for imaging CB1 receptors in patients with Tourette syndrome and Parkinson's disease (21). Other potential applications are in schizophrenia and depression, where CB1 receptors are upregulated in the frontal cortex (37–40). An emerging application of CB1 antagonists for obesity treatment and recent evidence that hypothalamic levels of endocannabinoids are raised in animal obesity models may promote PET of the CB1 system for development of drugs for treatment of obesity (2).

CONCLUSION

^{11}C -JHU75528 readily enters the mouse and baboon brain. ^{11}C -JHU75528 specifically and selectively labels cerebral CB1 receptors with substantially a higher value of the target-to-nontarget ratio than that of the previously reported radiotracers. The specific binding of ^{11}C -JHU75528 *in vivo* can be saturated by preinjection of nonlabeled JHU75528. Rimonabant, a selective CB1 antagonist and emerging medication for treatment of obesity and drug dependence, effectively blocks the specific binding of ^{11}C -JHU75528, whereas various central noncannabinoid drugs do not reduce normalized regional ^{11}C -JHU75528 binding. Injection of blocking doses of JHU75528 and rimonabant did not cause measurable side effects in mice or a baboon. ^{11}C -JHU75528 undergoes metabolism at a moderate rate and forms several hydrophilic metabolites, but only a minute fraction of metabolic radioactivity penetrates the BBB. Preliminary kinetic analyses of baboon PET images demonstrated reasonable values of BP in CB1-rich brain regions in baseline studies and substantially lower BP in the blocking study. ^{11}C -JHU75528 holds promise as a radiotracer with good imaging properties for quantification of CB1 receptors in the human brain.

ACKNOWLEDGMENTS

The authors thank Paige Finley for her help with the animal experiments, Robert C. Smoot for radiochemistry assistance, and David J. Clough and Karen Edmonds for PET scanner operation. We are grateful to Ayon Nandi and Lauren Smith for administrative assistance and Judy W. Buchanan and Elena Y. Barskiy for editorial help. This

research was supported by the Department of Radiology of Johns Hopkins University School of Medicine and U.S. Public Health Service grants from the National Institutes of Health (K24 DA00412, R01 NS38927, and R01 AA12839).

REFERENCES

1. Howlett AC, Barth F, Bonner TI, et al. International Union of Pharmacology. XXVII. classification of cannabinoid receptors. *Pharmacol Rev.* 2002;54:161–202.
2. Pertwee RG. The therapeutic potential of drugs that target cannabinoid receptors or modulate the tissue levels or actions of endocannabinoids. *AAPS J.* 2005;7:E625–E654.
3. Gambi F, De Berardis D, Sepede G, et al. Cannabinoid receptors and their relationships with neuropsychiatric disorders. *Int J Immunopathol Pharmacol.* 2005;18:15–19.
4. Witkin JM, Tzavara ET, Nomikos GG. A role for cannabinoid CB1 receptors in mood and anxiety disorders. *Behav Pharmacol.* 2005;16:315–331.
5. De Vries TJ, Schoffelmeier AN. Cannabinoid CB1 receptors control conditioned drug seeking. *Trends Pharmacol Sci.* 2005;26:420–426.
6. Le Foll B, Goldberg SR. Control of the reinforcing effects of nicotine by associated environmental stimuli in animals and humans. *Trends Pharmacol Sci.* 2005;26:287–293.
7. Vickers SP, Kennett GA. Cannabinoids and the regulation of ingestive behaviour. *Curr Drug Targets.* 2005;6:215–223.
8. Rinaldi-Carmona M, Barth F, Heaulme M, et al. SR141716A, a potent and selective antagonist of the brain cannabinoid receptor. *FEBS Lett.* 1994;350:240–244.
9. Van Gaal LF, Rissanen AM, Scheen AJ, Ziegler O, Rossner S. Effects of the cannabinoid-1 receptor blocker rimonabant on weight reduction and cardiovascular risk factors in overweight patients: 1-year experience from the RIO-Europe study. *Lancet.* 2005;365:1389–1397.
10. Cleland JG, Ghosh J, Freemantle N, et al. Clinical trials update and cumulative meta-analyses from the American College of Cardiology: WATCH, SCD-HeFT, DINAMIT, CASINO, INSPIRE, STRATUS-US, RIO-lipids and cardiac resynchronisation therapy in heart failure. *Eur J Heart Fail.* 2004;6:501–508.
11. Charalambous A, Marciniak G, Shiue CY, et al. PET studies in the primate brain and biodistribution in mice using (-)-5'-18 F- Δ^9 -THC. *Pharmacol Biochem Behav.* 1991;40:503–507.
12. Mathews WB, Ravert HT, Musachio JL, et al. Synthesis of [¹⁸F] SR144385: a selective radioligand for positron emission tomographic studies of brain cannabinoid receptors. *J Labelled Compds Radiopharm.* 1999;42:589–596.
13. Mathews WB, Scheffel U, Finley P, et al. Biodistribution of [¹⁸F] SR144385 and [¹⁸F] SR147963: selective radioligands for positron emission tomographic studies of brain cannabinoid receptors. *Nucl Med Biol.* 2000;27:757–762.
14. Mathews WB, Scheffel U, Raueo PA, et al. Carbon-11 labeled radioligands for imaging brain cannabinoid receptors. *Nucl Med Biol.* 2002;29:671–677.
15. Katoch-Rouse R, Pavlova OA, Caulder T, Hoffman AF, Mukhin AG, Horti AG. Synthesis, structure-activity relationship, and evaluation of SR141716 analogues: development of central cannabinoid receptor ligands with lower lipophilicity. *J Med Chem.* 2003;46:642–645.
16. Willis PG, Katoch-Rouse R, Horti AG. Regioselective F-18 radiolabeling of AM694, a CB1 cannabinoid receptor ligand. *J Labelled Compds Radiopharm.* 2003;46:799–804.
17. Katoch-Rouse R, Horti AG. Synthesis of N-(piperidin-1-yl)-5-(4-methoxyphenyl)-1-(2-chlorophenyl)-4-[¹⁸F]fluoro-1H-pyrazole-3-carboxamide by nucleophilic [¹⁸F]fluorination: a PET radiotracer for studying CB1 cannabinoid receptors. *J Labelled Compds Radiopharm.* 2003;46:93–98.
18. Gatley SJ, Gifford AN, Ding Y-S, et al. Development of PET and SPECT radioligands for cannabinoid receptors. In: Makriyannis A, Biegel D, eds. *Drug Discovery Strategies and Methods.* New York, NY: Marcel Dekker, Inc.; 2004:129–146.
19. Gatley SJ, Lan R, Volkow ND, et al. Imaging the brain marijuana receptor: development of a radioligand that binds to cannabinoid CB1 receptors in vivo. *J Neurochem.* 1998;70:417–423.
20. Li Z, Gifford A, Liu Q, et al. Candidate PET radioligands for cannabinoid CB(1) receptors: [¹⁸F]AM5144 and related pyrazole compounds. *Nucl Med Biol.* 2005;32:361–366.
21. Berding G, Muller-Vahl K, Schneider U, et al. [¹²³I]AM281 single-photon emission computed tomography imaging of central cannabinoid CB(1) receptors before and after delta⁹-tetrahydrocannabinol therapy and whole-body scanning for assessment of radiation dose in Tourette patients. *Biol Psychiatry.* 2004;55:904–915.
22. Willis PG, Pavlova OA, Chefer SI, Vaupel DB, Mukhin AG, Horti AG. Synthesis and structure-activity relationship of a novel series of aminoalkylindoles with potential for imaging the neuronal cannabinoid receptor by positron emission tomography. *J Med Chem.* 2005;48:5813–5822.
23. Laruelle M, Slifstein M, Huang Y. Relationships between radiotracer properties and image quality in molecular imaging of the brain with positron emission tomography. *Mol Imaging Biol.* 2003;5:363–375.
24. Waterhouse RN. Determination of lipophilicity and its use as a predictor of blood-brain barrier penetration of molecular imaging agents. *Mol Imaging Biol.* 2003;5:376–389.
25. Katoch-Rouse R, Chefer SI, Pavlova OA, et al. Development of C-11-NIDA-41020: a potential radiotracer for studying cerebral cannabinoid receptors (CB1) by PET. Presented at: IX Symposium on the Medical Applications of Cyclotrons; May 25–28, 2002; Turku, Finland.
26. Clark DE. In silico prediction of blood-brain barrier permeation. *Drug Discov Today.* 2003;8:927–933.
27. Shire D, Calandra B, Bouaboula M, et al. Cannabinoid receptor interactions with the antagonists SR141716A and SR144528. *Life Sci.* 1999;65:627–635.
28. Fan H, Ravert HT, Holt D, Dannals RF, Horti AG. Synthesis of 1-(2,4-dichlorophenyl)-4-cyano-5-(4-[¹¹C]methoxyphenyl)-N-(piperidin-1-yl)-1H-pyrazole-3-carboxamide ([¹¹C]JHU75528) and 1-(2-bromophenyl)-4-cyano-5-(4-[¹¹C]methoxyphenyl)-N-(piperidin-1-yl)-1H-pyrazole-3-carboxamide ([¹¹C]JHU75575) as potential radioligands for PET imaging of cerebral cannabinoid receptor. *J Labelled Compds Radiopharm.* In press.
29. Kuwabara H, Cumming P, Reith J, et al. Human striatal L-dopa decarboxylase activity estimated in vivo using 6-[¹⁸F]fluoro-dopa and positron emission tomography: error analysis and application to normal subjects. *J Cereb Blood Flow Metab.* 1993;13:43–56.
30. Wong DF, Yung B, Dannals RF, et al. In vivo imaging of baboon and human dopamine transporters by positron emission tomography using [¹¹C]WIN 35, 428. *Synapse.* 1993;15:130–142.
31. Ichise M, Liow JS, Lu JQ, et al. Linearized reference tissue parametric imaging methods: application to [¹¹C]DASB positron emission tomography studies of the serotonin transporter in human brain. *J Cereb Blood Flow Metab.* 2003;23:1096–1112.
32. Hilton J, Yokoi F, Dannals RF, Ravert HT, Szabo Z, Wong DF. Column-switching HPLC for the analysis of plasma in PET imaging studies. *Nucl Med Biol.* 2000;27:627–630.
33. Glass M, Dragunow M, Faull RL. Cannabinoid receptors in the human brain: a detailed anatomical and quantitative autoradiographic study in the fetal, neonatal and adult human brain. *Neuroscience.* 1997;77:299–318.
34. Herkenham M, Lynn AB, Little MD, et al. Cannabinoid receptor localization in brain. *Proc Natl Acad Sci U S A.* 1990;87:1932–1936.
35. Di Marco A, Yao D, Laufer R. Demethylation of radiolabelled dextromethorphan in rat microsomes and intact hepatocytes. *Eur J Biochem.* 2003;270:3768–3777.
36. Johnson DC, Hoop B, Kazemi H. Movement of CO₂ and HCO₃⁻ from blood to brain in dogs. *J Appl Physiol.* 1983;54:989–996.
37. Zavitsanou K, Garrick T, Huang XF. Selective antagonist [³H]SR141716A binding to cannabinoid CB1 receptors is increased in the anterior cingulate cortex in schizophrenia. *Prog Neuropsychopharmacol Biol Psychiatry.* 2004;28:355–360.
38. Ujike H, Morita Y. New perspectives in the studies on endocannabinoid and cannabis: cannabinoid receptors and schizophrenia. *J Pharmacol Sci.* 2004;96:376–381.
39. Hungund BL, Vinod KY, Kassir SA, et al. Upregulation of CB1 receptors and agonist-stimulated [³⁵S]GTPgammaS binding in the prefrontal cortex of depressed suicide victims. *Mol Psychiatry.* 2004;9:184–190.
40. Vinod KY, Arango V, Xie S, et al. Elevated levels of endocannabinoids and CB1 receptor-mediated G-protein signaling in the prefrontal cortex of alcoholic suicide victims. *Biol Psychiatry.* 2005;57:480–486.